Naval Research Laboratory

Washington, DC 20375-5320

NRL/MR/6794--96-7789

Test Particle Calculation of Electric Currents In Magnetic Field-Reversed Regions

J. CHEN

Beam Physics Branch
Plasma Physics Division

D.L. HOLLAND

Department of Physics, Illinois State University
Normal, IL

April 3, 1996

REPORT DOCUMENTATION PAGE

Form Approved
OMB No. 0704-0188

1. AGENCY USE ONLY (*Leave Blank*)	2. REPORT DATE	3. REPORT TYPE AND DATES COVERED
	April 3, 1996	Interim

4. TITLE AND SUBTITLE

Test Particle Calculation of Electric Currents In Magnetic Field-Reversed Regions

5. FUNDING NUMBERS

PE - 67-3788-05

6. AUTHOR(S)

D.L. Holland,* and J. Chen

7. PERFORMING ORGANIZATION NAME(S) AND ADDRESS(ES)

Naval Research Laboratory
Washington, DC 20375-5320

8. PERFORMING ORGANIZATION REPORT NUMBER

NRL/MR/6794--96-7789

9. SPONSORING/MONITORING AGENCY NAME(S) AND ADDRESS(ES)

Office of Naval Research
800 North Quincy Street
Arlington, VA 22217-5660

NASA
Washington, DC 20546

10. SPONSORING/MONITORING AGENCY REPORT NUMBER

11. SUPPLEMENTARY NOTES

*Illinois State University, Normal, IL 61790-4560

12a. DISTRIBUTION/AVAILABILITY STATEMENT

Approved for public release; distribution unlimited.

12b. DISTRIBUTION CODE

13. ABSTRACT (*Maximum 200 words*)

A wide range of important plasma phenomena can take place in boundary layers between regions of oppositely directed magnetic fields where collisionless particles can execute magnetized and unmagnetized motion sequentially. Much work has been done recently to study such phenomena in space physics settings using test particle simulations. An important quantity in such systems is the electric current carried by charged particles, since it is this current which must produce the field reversal. Additionally one must calculate the particle density and pressure tensor in order to verify the existence of self-consistent equilibria. We present in this paper an algorithm for evaluating self-consistent Vlasov equilibria in magnetic field-reversed regions. In addition, we describe a technique to separate the magnetic field into the contribution due to the plasma diamagnetism, $4\pi M$, and the part due to the actual particle current, H.

14. SUBJECT TERMS

Nonlinear particle dynamics
Magnetosphere
Test particle
Simulations

15. NUMBER OF PAGES

29

16. PRICE CODE

17. SECURITY CLASSIFICATION OF REPORT	18. SECURITY CLASSIFICATION OF THIS PAGE	19. SECURITY CLASSIFICATION OF ABSTRACT	20. LIMITATION OF ABSTRACT
UNCLASSIFIED	UNCLASSIFIED	UNCLASSIFIED	UL

CONTENTS

TEST PARTICLE CALCULATION OF ELECTRIC CURRENTS IN MAGNETIC FIELD-REVERSED REGIONS

I. INTRODUCTION

Many naturally occurring systems can be thought of as boundary regions between oppositely directed magnetic fields, where the dominant magnetic component of the magnetic field reverses sign and where "current sheets" are formed. Such field reversal regions occur in laboratory as well as astrophysical plasmas, and important physical phenomena such as reconnection can take place.

In space and astrophysical plasmas, the charged particles are usually collisionless. A simple example of a field reversal which models the Earth's magnetotail is the quasi-neutral sheet shown in Figure 1. The x-component of the magnetic field, $B_x(z)$, reverses sign at $z = 0$. The particle motion in this system is nonadiabatic [1] and has been shown to undergo chaotic scattering [2,3]. Another example of a field reversed geometry is given in Figure 2. Here there is an X–type neutral line at $x = 0$ and $z = 0$, where the magnetic field vanishes. The particle motion near an X–line is also chaotic [4,5].

Because of the chaotic particle motion, the properties of plasmas in regions containing current sheets are nontrivial to study. An approach that has been fruitful is to use test particle simulations in which the charged particle motion is integrated in prescribed fields [6-13]. Although such simulations do not contain complete physical interactions, the results have often been successful in explaining observed satellite data [7,10].

A key property of magnetic field reversals is the electric current profile which determines the magnetic field, the magnetic energy distribution, and particle distribution function, the last representing the internal and free energy distribution of the plasma. Issues concerning current distributions have been investigated using test-particle simulations [13-19, 25]. For example, *Burkhart et al.* [14] modeled the structure of the "dissipation" region in collisionless reconnection. In this work, the current was calculated by following a distribution of particles through a prescribed field. Using the calculated current, a new magnetic field is calculated. The process was iterated until Ampere's law is satisfied. In some recent papers, self-consistent equilibrium current sheets have been computed in the magnetotail geometry [15,17,18]. In these works, the cross-tail current density is again constructed by binning the contributions from each test particle using a rectangular (Cartesian) grid and is iterated until self-consistency is achieved. The particle orbits are computed directly from the equation of motion.

An important feature of the particle motion in and near field reversals is that a given particle orbit consists of alternating segments of magnetized and unmagnetized motion [1]. A field reversal thus can be divided into spatial regions according to the type of particle motion. Consider a particle of energy $H = mv^2/2$. It is nearly unmagnetized while in the region $|z| \lesssim d_j \equiv (\rho_z L)^{1/2}$, where ρ_z is the particles gyroradius in the z-component of the magnetic field and L is the scale length of the reversal region in the x-component of the magnetic field, and it is magnetized for $|z| \gtrsim d_j$ [17].

In this report, we examine in detail the process of numerically computing electric currents in systems in which the particle motion alternately undergoes magnetized and unmagnetized motion. In addition, we describe an algorithm for approximately separating the magnetic field

Manuscript approved November 15, 1995.

into the part due to the plasmas diamagnetism, $4\pi\mathbf{M}$, and the part due to the actual particle current, $\mathbf{H}$.

II. Single Particles

In test particle simulations, particle motion is computed in prescribed fields. The resulting equilibrium profiles (i.e., electric currents, particle density, and pressure tensor) can then be used to calculate the fields, which in turn may be used as a new prescribed field in the test particle simulation. This process may be iterated to self-consistency. Hence, a fundamental step is to compute the contribution of each particle to the equilibrium profiles in a given field. At any given time the distribution which represents a single particle is formally given by

$$f_{sp}(\mathbf{r},\mathbf{v},t) = \frac{1}{L^6\Omega_0^3}\,\delta\Big(\frac{\mathbf{r}-\mathbf{r}(t)}{L}\Big)\delta\Big(\frac{\mathbf{v}-\mathbf{v}(t)}{\Omega_0 L}\Big). \tag{1}$$

Here L is a characteristic scale length for the system and Ω_0 is a characteristic frequency. Typically, computation of physical quantities is carried out using Cartesian coordinates where we have

$$\delta\Big(\frac{\mathbf{r}-\mathbf{r}(t)}{L}\Big) = \delta\Big(\frac{x-x(t)}{L}\Big)\delta\Big(\frac{y-y(t)}{L}\Big)\delta\Big(\frac{z-z(t)}{L}\Big) \tag{2a}$$

and

$$\delta\Big(\frac{\mathbf{v}-\mathbf{v}(t)}{\Omega_0 L}\Big) = \delta\Big(\frac{v_x-v_x(t)}{\Omega_0 L}\Big)\delta\Big(\frac{v_y-v_y(t)}{\Omega_0 L}\Big)\delta\Big(\frac{v_z-v_z(t)}{\Omega_0 L}\Big). \tag{2b}$$

The instantaneous particle and current densities are found by evaluating the zeroth and first velocity moments of f_{sp}, i.e. $n(\mathbf{r},t) = \int d\mathbf{v}\, f(\mathbf{r},\mathbf{v},t)$ and $\mathbf{j}(\mathbf{r},t) = qn(\mathbf{r},t)\mathbf{U}(\mathbf{r},t) = q\int d\mathbf{v}\,\mathbf{v}\, f(\mathbf{r},\mathbf{v},t)$. Defining the normalized variables $\hat{\mathbf{r}} = \mathbf{r}/L$ and $\hat{\mathbf{v}} = \mathbf{v}/(\Omega_0 L)$, these become

$$n(\hat{\mathbf{r}},t) = \frac{1}{L^3}\delta[\hat{\mathbf{r}}-\hat{\mathbf{r}}(t)] \tag{3a}$$

and

$$\mathbf{j}(\hat{\mathbf{r}},t) = \frac{q\Omega_0}{L^2}\hat{\mathbf{v}}(t)\,\delta[\hat{\mathbf{r}}-\hat{\mathbf{r}}(t)]. \tag{3b}$$

Instead of evaluating the pressure tensor $\mathbf{p}(\mathbf{r},t) = m\int d\mathbf{v}\,(\mathbf{v}-\mathbf{U})(\mathbf{v}-\mathbf{U})\,f(\mathbf{r},\mathbf{v},t)$, we calculate the second velocity moment of f_{sp}, i.e. $\mathbf{q}(\mathbf{r},t) = m\int d\mathbf{v}\,\mathbf{v}\mathbf{v}\,f(\mathbf{r},\mathbf{v},t)$, since this does not require *a priori* knowledge of the average flow velocity $\mathbf{U}$. Evaluating this integral, we find

$$\mathbf{q}(\hat{\mathbf{r}},t) = \frac{m\Omega_0{}^2}{L}\hat{\mathbf{v}}(t)\hat{\mathbf{v}}(t)\,\delta[\hat{\mathbf{r}}-\hat{\mathbf{r}}(t)]. \tag{3c}$$

It is trivial to show that $\mathbf{q}$ may be written in terms of $\mathbf{p}$, $\mathbf{j}$, and n as,

$$\mathbf{q} = \mathbf{p} + (m/q^2 n)\mathbf{j}\mathbf{j}.$$

(With this relation in mind, we shall henceforth simply refer to $\mathbf{q}$ as the pressure unless otherwise stated.)

In a standard particle in cell code it is the instantaneous density and current which is distributed onto a grid for each particle at every time step [20]. The resulting total density and current is then used to calculate updated fields which are used to "push" the particles for the next time step. In self-consistent test particle simulations, on the other hand, a particle is "pushed" through the system in a prescribed field from its point of injection to its point of escape. After "pushing" all of the particles in a source distribution through the system, the average currents and densities each particle contributes while in the system are added together to determine the total current and density which are then used to update the fields. Thus, the test particle code is very well suited for determining time stationary solutions with very good spatial resolution using a relatively small number of particles. By its very nature, however, it can only yield information regarding time evolution in the sense of a series of quasistatic equilibria.

The contribution of a single particle to the equilibrium quantities is obtained by averaging the values of those quantities along the trajectory for the time T the particle is in the system *i.e.*

$$\bar{n}(\hat{\mathbf{r}}) = \frac{1}{T}\int_0^T n(\hat{\mathbf{r}},t)dt \tag{4a}$$

$$\bar{\mathbf{j}}(\hat{\mathbf{r}}) = \frac{1}{T}\int_0^T \mathbf{j}(\hat{\mathbf{r}},t)dt. \tag{4b}$$

$$\bar{\mathbf{q}}(\hat{\mathbf{r}}) = \frac{1}{T}\int_0^T \mathbf{q}(\hat{\mathbf{r}},t)dt. \tag{4c}$$

(Note that the value of T will in general be different for each particle.) If we assume that the particle phase space information (i.e. position and velocity) are known at the evenly spaced time intervals, $t_n = n\Delta t$, where $0 < n < N$ and $N\Delta t = T$, we may approximate the integral in (4a) as a finite sum. Hence the average single particle density becomes

$$\bar{n}(\hat{\mathbf{r}}) = \frac{1}{L^3}\mathbf{D}(\hat{\mathbf{r}}) = \frac{1}{L^3}\left[\frac{1}{N}\sum_{n=0}^{N}\delta_{\hat{\mathbf{r}},\hat{\mathbf{r}}_n}\right]. \tag{5a}$$

Here $\delta_{\hat{\mathbf{r}},\hat{\mathbf{r}}_n}$ is the Kroneker delta function, $\hat{\mathbf{r}}_n = \hat{\mathbf{r}}(n\Delta t)$ and $\mathbf{D}(\hat{\mathbf{r}})$ is the normalized single particle density. In a similar manner, the average current density and pressure which may be attributed to a single particle may be written as

$$\bar{\mathbf{j}}(\hat{\mathbf{r}}) = \frac{q\Omega_0}{L^2}\mathbf{J}(\hat{\mathbf{r}}) = \frac{q\Omega_0}{L^2}\left[\frac{1}{N}\sum_{n=0}^{N}\hat{\mathbf{v}}(n\Delta t)\delta_{\hat{\mathbf{r}},\hat{\mathbf{r}}_n}\right]. \tag{5b}$$

$$\bar{\mathbf{q}}(\hat{\mathbf{r}}) = \frac{m{\Omega_0}^2}{L}\mathbf{Q}(\hat{\mathbf{r}}) = \frac{q{\Omega_0}^2}{L}\left[\frac{1}{N}\sum_{n=0}^{N}\hat{\mathbf{v}}(n\Delta t)\hat{\mathbf{v}}(n\Delta t)\delta_{\hat{\mathbf{r}},\hat{\mathbf{r}}_n}\right]. \tag{5c}$$

Where $\mathbf{J}(\hat{\mathbf{r}})$, and $\mathbf{Q}(\hat{\mathbf{r}})$ are the normalized single particle current density and pressure tensor profiles respectively. Using (5) it is a trivial matter to distribute the single particle density and current onto a grid. In essence, by using the above technique, we are relating average residence times of particles in a region to equilibrium profiles.

As a concrete example, we consider particle motion in the modified Harris model of the Earth's magnetotail $\mathbf{B} = B_0 \tanh(z/L)\,\hat{\mathbf{x}} + B_z\,\hat{\mathbf{z}}$ (Fig. 1). Here B_0 is the asymptotic value of the field due to the current sheet, L is the characteristic scale length of the field reversal, B_z is a constant magnetic field normal to the current sheet, and $\hat{\mathbf{x}}$ is in the sunward direction. The particle motion in this geometry is well documented. (A review can be found in reference [17].) Since the fields in the modified Harris model are translationally invariant in the x and y directions, we need only consider variations in the z-direction when calculating the current and density profiles. Similar techniques may be used for X-line geometries (Figure 2), however, in that case we must use a two-dimensional grid since there is variation in both the x and z directions.

Assume that we wish to distribute the current and density profiles onto a one dimensional grid in the z direction with $M+1$ equally spaced points between $\pm\hat{z}_{max}$. If on the n^{th} time step, the particle falls between the m^{th} and $(m+1)^{th}$ grid points, we use a linear interpolation scheme to distribute the Kroneker delta weight function onto the grid, i.e. we add to the density and current at each of these points the amounts

$$\Delta n(\hat{z}_m) = \frac{|\hat{z}_m - \hat{z}|}{\Delta\hat{z}} \tag{6a}$$

$$\Delta n(\hat{z}_{m+1}) = \frac{|\hat{z}_{m+1} - \hat{z}|}{\Delta\hat{z}} \tag{6b}$$

$$\Delta\mathbf{j}(\hat{z}_m) = \hat{\mathbf{v}}(n\Delta t)\frac{|\hat{z}_m - \hat{z}|}{\Delta\hat{z}} \tag{6c}$$

$$\Delta\mathbf{j}(\hat{z}_{m+1}) = \hat{\mathbf{v}}(n\Delta t)\frac{|\hat{z}_{m+1} - \hat{z}|}{\Delta\hat{z}} \tag{6d}$$

$$\Delta\mathbf{q}(\hat{z}_m) = \hat{\mathbf{v}}(n\Delta t)\hat{\mathbf{v}}(n\Delta t)\frac{|\hat{z}_m - \hat{z}|}{\Delta\hat{z}} \tag{6e}$$

$$\Delta\mathbf{q}(\hat{z}_{m+1}) = \hat{\mathbf{v}}(n\Delta t)\hat{\mathbf{v}}(n\Delta t)\frac{|\hat{z}_{m+1} - \hat{z}|}{\Delta\hat{z}} \tag{6f}$$

Here we have defined $\Delta\hat{z} = 2\hat{z}_{max}/M$. This procedure is followed so long as the particle position falls between $\pm z_{max}$. Of course, if we are to use the top (bottom) grid point, we must use a guard cell, *i.e.*, if the particle lies between $\hat{z}_{max}$ and $\hat{z}_{max} + \Delta z$, ($-\hat{z}_{max}$ and $-\hat{z}_{max} - \Delta z$) we must add to the density, current and pressure at the top (bottom) point amounts equal to (6a),(6c) and (6e) ((6b),(6d) and (6f)) where now $\hat{z}_m = \hat{z}_M$ ($\hat{z}_{m+1} = \hat{z}_1$). Finally, in order to insure unit probability of finding the particle in the system, all quantities are normalized such that the height integrated density (i.e. the sum over the $\mathbf{D}(\hat{z})$ contributions at each grid point) is equal to one.

III. PARTICLE DISTRIBUTIONS

Having found the equilibrium profiles due to a single particle moving through the field reversal region, we now wish to weight these single particles in such a fashion as to model a source distribution of particles. In this context there is some ambiguity as to how to perform the reconstruction based on what is assumed to be known. Here we shall discuss two possible normalization options. In both cases, we assume that each particle represents a unit volume of phase space and we launch shells of constant energy and reconstruct the source distribution by properly weighting the shells. The difference between the two normalization schemes arise in how we weight the particles on a given energy shell.

In the first scenario, (which is the more general of the two) we assume that we know the density of the incoming distribution and that the density of the outgoing distribution is determined by the particle dynamics. In this case, we calculate the density a given particle gives to the top grid cell when it is initially approaching the midplane (assuming the particle is launched from above the field reversal region) and normalize the density for that particle such that this contribution is unity. Note that this normalization implies that if a particle leaves from the bottom of the current calculation region, the density of the top cell will be unity. If the particle leaves from the top, however, the density of the top cell will be greater than unity. Once we have calculated the density and current for each of the particles on a given energy shell, all of the single particle densities and currents are added together and divided by the total number of particles that enter into the density calculation region for that shell. Note that in this scenario, we may either symmetrize the current sheet by assuming equal particle sources above and below the midplane, or we may launch separate distributions from each source region.

In the second technique, we assume *a priori* that the particle sources are symmetric and that we only know the total density which a particle contributes to the top grid cell is equal to unity. In this case we symmetrize the single particle density and current before normalizing them. The single particle equilibrium profiles are then normalized such that the density in the top grid cell is unity. (Note that this now includes particles that are entering and leaving the system in the normalization.) The single particles profiles for a given energy shell are added together and divided by the total number of particles which enter the current calculation region for that shell.

In general the first technique is preferable since it reduces the number of assumptions made in the analysis. Computationally it is much more difficult, however, since we must keep track of the particle while it is initially approaching the midplane and make a determination as to when to cut off the calculation of the normalization factor (*i.e.* how many counts the particle contributes to the top grid cell.)

For either technique, once we have calculated the current contribution for each shell, we normalize the profiles by their relative phase space volumes. This is done so that we do not need to space the shells equally in velocity. For example, suppose we have P energy levels between $\hat{H} = \hat{H}_{min}$ and $\hat{H} = \hat{H}_{max}$. The p^{th} shell is then taken to represent the phase space volume $(v_p - v_{p-1})/v_{max}$, where $\hat{H} = \frac{1}{2}mv^2$ and $p = 1, 2, \ldots, P$. The phase space volume

represented by the first shell is simply v_1/v_{max}. Note that in this weighting scheme the sum of all of the shells has unit weight. Finally the shells are weighed by the desired model velocity distribution function, (*e.g.* Maxwellian, Kappa, etc.) and summed together to produce the total density and current for the assumed particles sources.

IV. Application to the Magnetotail

In the case of the magnetotail, we are primarily interested in the y-component of the current, since this is the component which produces the x-component of the magnetic field, i.e. the field reversal. Using the calculated current, we compute an updated magnetic field which we then use as the input field. For the one-dimensional case discussed here, the magnetic field is calculated by numerically integrating the calculated y-current profile in the z-direction with the numerical constant found by requiring the magnetic field to vanish at the midplane. (For a two-dimensional case such as the X-line geometry, it is simpler to solve for the vector potential using a two-dimensional Poisson solver.) In updating the magnetic field, we have employed an overall weighting factor on the current and density so as to insure that the amplitude of the asymptotic magnetic field remains unchanged. The process is iterated until the input and calculated field profiles have converged.

Recently it has been found that if all three components of the current are kept, an antisymmetric y-component of the magnetic field grows until its peak value is on the order of the x-component [21-23]. This field is believed to be the test particle code (time independent) analog of a wave which has been shown to develop in the current sheet using time dependent hybrid simulations [23]. For the purpose of our discussion here, it suffices to note that if the source distribution of particles is highly field aligned, this wave has a fast growth rate and saturates, with B_y on the order of B_x. For more isotropic source distributions, it was found that the growth rate is much slower (on the order of half an hour for magnetotail parameters) and saturated with a much smaller amplitude [23]. Thus, it only makes sense to use the test particle formulation for calculating equilibria for the cases in which we have a nearly isotropic source of particles. (It is also important to note that in order to successfully run the hybrid simulation, one needs to input the self-consistent magnetic field structure calculated using the test particle code. If this is not done, the hybrid simulation starts too far from equilibrium which results in too much free energy for wave growth and a resulting disruption of the equilibrium.) Henceforth, we will suppress the y-component of the magnetic field and use only source distributions that produce small B_y.

To compare out results with observed quantities, we must convert our simulation results into physically meaningful units. Using equations (5a-c), we see that the total particle density, current density and pressure may be written as

$$\bar{n}_{tot}(\hat{z}) = \frac{\eta}{L^3}\sum_{i=1}^{N_p} C_i \mathbf{D}_i(\hat{z}) = \frac{\eta}{L^3}\mathbf{D}_{tot}(\hat{z}), \qquad (7a)$$

$$\bar{\mathbf{j}}_{tot}(\hat{z}) = \frac{\eta q \Omega_0}{L^2} \sum_{i=1}^{N_p} C_i \mathbf{J}_i(\hat{\mathbf{z}}) = \frac{\eta q \Omega_0}{L^2} \mathbf{J}_{tot}(\hat{z}) \tag{7b}$$

$$\bar{\mathbf{p}}_{tot}(\hat{z}) = \frac{\eta m \Omega_0^2}{L} \sum_{i=1}^{N_p} C_i \mathbf{P}_i(\hat{\mathbf{z}}) = \frac{\eta m \Omega_0^2}{L} \mathbf{P}_{tot}(\hat{z}) \tag{7c}$$

where C_i is the weighting applied to the i^{th} particle density, N_p is the number of particles used and η is an overall weighting factor used to ensure a constant asymptotic magnetic field strength. We now need to relate η, L and our dimensionless density, current, and pressure to measured values of the asymptotic magnetic field and density.

From Ampere's law, the asymptotic value of the magnetic field may be related to the height integrated current through the relation

$$2B_0 = \mu_0 \frac{\eta q \Omega_0}{L} \int_{-\infty}^{+\infty} \mathbf{J}_{tot}(\hat{z})(dz/L) \tag{8}$$

In our computational algorithm, we wish to we maintain a constant magnitude for the asymptotic magnetic field (*i.e.*, $B(-\infty)/B_0 = -1$ and $B(+\infty)/B_0 = +1$). and hence we require

$$\int_{-\infty}^{+\infty} \mathbf{J}_{tot}(\hat{z})(dz/L) = 2 \tag{9}$$

Substituting (9) into (8) we find that the amplitude of the magnetic is given by

$$B_0 = 4\pi \times 10^2 \frac{\eta q \Omega_0}{L} \text{nT} \tag{10}$$

or equivalently, since Ω_0 is proportional to B_0 we find that

$$\eta/L = 5.19 \times 10^{16} \frac{\mu}{Z^2} \text{m}^{-1} \tag{11}$$

where μ is the ratio of the ion to the proton mass and Z is the charge state of the ion. Thus we have a relationship between the simulation quantities η/L and physically determined quantities. (Typically we assume that the ions are protons so that $\mu = Z = 1$.)

From equation (7a) we know that the asymptotic density (or alternatively the density in the top cell) is given by

$$\bar{n}_{tot}(\hat{z}_{max}) = \frac{\eta}{L^3} \mathbf{D}_{tot}(\hat{z}_{max})$$

where z_{max} is the maximum value of the normalized position. If we require that $\bar{n}_{tot}(\hat{z}_{max}) = n_0$ where n_0 is the physical particle density given in particles per cubic centimeter, we find that

$$\frac{\eta}{L^3} = \frac{n_0}{\mathbf{D}_{tot}(\hat{z}_{max})} \tag{12}$$

where $\mathbf{D}_{tot}(\hat{z}_{max})$ is the computed density in the top grid cell (output from the code). Hence we have a relationship between the physically measured particle density and the ratio of the simulation quantities η/L^3 and $\mathbf{D}_{tot}(\hat{z}_{max})$. From equations (11) and (12) it is now possible to uniquely determine the values of η and L separately for any given physical situation.

In space physics it is often useful to give distances in terms of earths radii ($R_E = 6.37\times10^6$m). To do this we write $L = \sigma R_E$, and hence from (11) we have

$$\eta/\sigma = 3.307 \times 10^{23}\frac{\mu}{Z^2}$$

and from (12) we have that

$$\frac{\eta}{\sigma^3} = \frac{n_0}{\mathbf{D}_{tot}(\hat{z}_{max})}R_E^3$$

These equation may be solved for σ to obtain

$$\sigma = 0.036\sqrt{\frac{\mu n_0}{Z^2\mathbf{D}_{tot}(\hat{z}_{max})}} \tag{13}$$

In essence, equation (13) gives us the scale factor for changing from our simulation dimensions to the physical dimensions for a given particle density and ion species.

Using the above results it is now a trivial process to determine the numerical coefficients to convert our simulation density, current and pressure profiles into physically meaningful data, *i.e.*

$$\frac{\eta q\Omega_0}{L^2} = 0.125(B_0/\sigma)\,\mathrm{nA/m^2}. \tag{14}$$

and

$$\frac{\eta m{\Omega_0}^2}{L} = 7.97 \times 10^{-12}({B_0}^2)\,\mathrm{dyne/cm^2}. \tag{15}$$

In equations (13)-(15) B_0 is measured in nT and n_0 is measured in cm^{-3},

An additional quantity of interest is the normalized temperature, $\hat{T}$, of the distribution which is input to the code. This is related to the physical temperature, T, through the relation

$$\hat{T} = 2T/m{\Omega_0}^2L^2. \tag{16}$$

Solving for the physical temperature in keV, we find

$$T = 3.88{B_0}^2\sigma^2\hat{T}(Z^2/\mu)\,\mathrm{keV}. \tag{17}$$

In Figure 3 we give an example the self-consistent density, current, magnetic field and pressure profiles calculated using the above algorithm where we have assumed that the particle source is a kappa distribution ($\kappa = 4.5$) with a bulk drift in the tailward direction of 10% of the thermal velocity and a density of $0.5\mathrm{cm}^{-3}$, the asymptotic magnetic field is 20nT, and $B_z/B_0 = 0.1$.

To verify the existence of a self-consistent equilibrium, the density, current and pressure profiles must satisfy global pressure balance. In general this requirement is given by the first moment of the Vlasov equation which yields

$$\nabla \cdot \left(\mathbf{P} + mN\mathbf{U}\mathbf{U} + \frac{B^2}{8\pi}\mathbf{I} - \frac{\mathbf{B}\mathbf{B}}{4\pi}\right) = 0 \tag{18}$$

where we are using the actual pressure $\mathbf{P} = m\int d\mathbf{v}\,(\mathbf{v}-\mathbf{U})(\mathbf{v}-\mathbf{U})\,f(\mathbf{r},\mathbf{v})$, and as usual $N\mathbf{U} = \int d\mathbf{v}\,\mathbf{v}\,f(\mathbf{r},\mathbf{v})$ and $N = \int d\mathbf{v}\,f(\mathbf{r},\mathbf{v})$ are the particle flux and particle density and $\mathbf{I}$ is the unit matrix. In 1D with only $\partial/\partial z \neq 0$, Eq. (18) becomes

$$P_{xz} - \frac{B_x B_z}{4\pi} = const \tag{19a}$$

$$P_{yz} - \frac{B_y B_z}{4\pi} = const \tag{19b}$$

$$P_{zz} + \frac{{B_x}^2 + {B_y}^2 - {B_z}^2}{8\pi} = const. \tag{19c}$$

We have also used the continuity equation and the symmetry of the system to deduce that $NU_z = 0$. In Figure 4 we plot equations (19 a-c) for the case depicted in Figure 3. Note that all three equations are well satisfied.

V. Effects of Diamagnetism

An interesting aspect of the field reversed geometry is the effects of diamagnetism. Even though the density in the current sheet typically only varies by a few percent in the cases that produce small B_y, we find that it is in these cases that the plasma diamagnetism becomes a significant effect. This is because the particle executes magnetized motion for $|z| \gtrsim (\rho_z L)^{1/2}$, and unmagnetized motion for $|z| \lesssim (\rho_z L)^{1/2}$. When the particle motion changes character, it contributes a diamagnetic current in that region. As we will show, this diamagnetic current depends on the asymptotic pitch angle of the particles with larger pitch angles producing larger diamagnetic currents. In this section we will discuss the diamagnetic current due to an individual particle and then discuss the ramifications on distributions of particles.

Regardless of the intervening motion (*i.e.* chaotic or not), the shift in the y-component of the guiding center is given by

$$\Delta\hat{y}_{gc} = \sqrt{\frac{2{b_z}^2\hat{H}}{1+b_n^2}}\left[|\cos\beta_2| + |\cos\beta_1|\right] \tag{20}$$

where $b_z = B_z/B_0$ is the ratio of the z and x magnetic fields in the asymptotic region, $\hat{H} = H/m{\Omega_0}^2L^2$ is the normalized energy of the particle, $\Omega_0 = qB_0/mc$ is the cyclotron frequency in the x-component of the magnetic field, and β_1 (β_2) is the initial (final) pitch angle

of the particle as it enters (leaves) the system. From (20), we may calculate the average current density supplied by a particle to be

$$\langle \mathbf{j} \rangle = q\Delta y_{gc}/\Delta t \tag{21}$$

where Δt is the time required for the particle to enter and leave the current calculation region [24].

In Figure 5a we show the trajectory of a typical orbit and in Figure 5b we show the associated current profile in the y-direction between $\hat{z} = \pm 5$ as calculated using (6a)-(6d). A positive charge moves in the direction indicated by the arrow. The particle is launched from $\hat{z}_0 = 6$ with the energy $H = 0.24m\Omega_0{}^2L^2$, and an initial pitch angle of 100° (using the field conventions of Figure 1). In its interaction with the neutral sheet, here taken to be the time the particle is in the current calculation region ($|z| \leq 5$), the y-component of the particle guiding center in the asymptotic regions is shifted by an amount $\Delta y_{gc} = 3.03L$ in a time $482\Omega_0^{-1}$. This implies an average y-current density between $\hat{z} = \pm 5$ of $\langle \mathbf{j} \rangle = 6.28 \times 10^{-3}\, qL\Omega_0$. If we average the numerically calculated current density profile between $\hat{z} = \pm 5$, however, we obtain a net negative total current of $-5.5 \times 10^{-2}\, qL\Omega_0$. This somewhat surprising result of a net negative current density is caused by the plasma's diamagnetism and as we shall see is strongly dependent on the asymptotic pitch angle of the particle.

To understand the difference between the numerically computed average current density and the value given by $q\Delta y_{gc}/\Delta t$ the size of the current calculation region is increased to $\hat{z} \leq \pm 8$ so that the particle is in the calculation region through out its entire orbit. We have calculated the J_y profile using equations (6a)-(6d) at several times to see how the current is deposited onto the grid. Figure 6 shows the result at three times: (a) $T = 200\Omega_0^{-1}$, (b) $T = 400\Omega_0^{-1}$, and (c) $T = 600\Omega_0^{-1}$. The important feature to note in these figures is the development of current peaks in regions associated not with any shift in the y-component of the guiding center, but rather with the injection and exit points of the particles. If these peaks are included in the numerically calculated average current, the net magnitude of the current density is positive and in agreement with the value calculated from $\langle \mathbf{j} \rangle = q\Delta y_{gc}/\Delta t$. Since the total average current (including the peaks at the entry and exit points) is in agreement with the expected value, this implies we have deposited a net negative current in the midplane which exactly cancels the positive current at the entry and exit points. This negative current in the field reversal region is in addition to the positive current due to the meandering motion of the ion.

The formation of the positive current peaks at the entry and exit points and the deposition of negative currents near the midplane may be intuitively understood if we examine a plot of $\hat{v}_y$ *vs.* $\hat{z}$ (Figure 7a). If we suppose that we are putting the current into bins of width L, then it is clear that the finite gyroradius effects in the regions where the guiding center is well defined (*i.e.* from points a to b and from points c to d) produce a net positive current in the top and bottom grid cells but tend to leave net negative current near the midplane.

Another way of understanding the development of the current peaks at the entry and exit sites is to examine the case where B_z goes to zero. Here the magnetic field is purely in the

x-direction but we are still griding the current as a function of z (Figure 8). Examining Figure 8, we see that for grid cells above the particle guiding center there are only positive contributions to the y-current density, whereas below the guiding center there are only negative contributions to the y-current density. Thus, we would expect to develop a positive current peak above the guiding center position and a negative current peak of equal magnitude below the guiding center position. If the two peaks are added together, we obtain the physically reasonable result of no net current in the y-direction. The same difficulties do not apply to the x-current density since it has equal positive and negative contributions both above and below the particle guiding center. (This formation of equal and opposite current peaks above and below the guiding center is nothing more than the one-dimensional manifestation of the particles diamagnetism.) If we now allow for finite B_z, the same general effects will occur in the asymptotic regions (*i.e.* far from the midplane), but now the peaks will tend to separate as we let T increase since the particles are now moving down the field line. This effect is illustrated in Figure 6a where we have two equal and opposite current peaks separated by a region of zero current. At the time depicted in the Figure 6a, the particle was always in the asymptotic region where the magnetic field is essentially constant.

In appendix A, we show that the net positive y-velocity deposited around the entry and exit point (or conversely the net negative y-velocity deposited near the midplane) for a particle may be approximated by

$$\langle \hat{v}_y \rangle_p \approx 4 \sqrt{\frac{2\hat{H}}{1+{b_z}^2}} \sin\beta \sum_{k=0}^{K} \sqrt{1 - \left(\frac{2\pi k b_n \cot\beta}{\sqrt{1+{b_z}^2}} \right)^2} \qquad (22a)$$

where

$$K = \mathrm{Int}\left[\frac{\sqrt{1+{b_z}^2}}{2\pi b_z} \tan\beta \right] \qquad (22b)$$

The quantity $\langle \hat{v}_y \rangle_p$ is related to the current density in the peak through the relation $\langle \hat{v}_y \rangle_p = T \langle j_y \rangle_p$ where T is the total time between when the particle is injected into, and when it leaves the current calculation region. Figures 9a–9c are plots of the approximate analytic expression (solid line) for $\langle \hat{v}_y \rangle_p$ as a function of the pitch angle for $\hat{H} = 1.0$ and (a) $b_n = 0.1$, (b) $b_n = 0.2$ and (c) $b_n = 0.4$. The points (•) are numerically evaluated by "pushing" the particle through the assumed field and keeping track of the y-velocity deposited around the entry point of the particle. We note that for nearly field aligned particles the value of $\langle \hat{v}_y \rangle_p$ is small thus indicating that there is only a small diamagnetic current. For pitch angles near 90°, however, there is substantial diamagnetic current in all cases. The agreement between the analytical and the numerical results is in good agreement throughout the parameter space. Note the breaks in both the theoretical and numerical curves. Except for a phase shift which is easily understood in terms of the approximations made in the derivation of the theoretical expression, the locations and number of breaks are in good agreement with the numerical results (*cf.* Appendix A).

It is interesting to estimate the critical pitch angle, β_c, at which the negative diamagnetic current deposited in the vicinity of the midplane is equal to the positive current due to the meandering motion of the particle in the field reversal region (*i.e.* the pitch-angle at which the net current supplied by the ion is in the wrong direction to aid in the production of the field reversal). As a lowest order approximation, we assume that as the particle crosses the midplane all of its energy is in the y-direction and that it remains in the vicinity of the midplane for one half of a cyclotron orbit in the z-component of the magnetic field [24]. (Note that this is actually an over estimate of the meandering motion current since not all of the energy will be in y-direction.) This implies that the net y-velocity deposited near the midplane due to the meandering motion may be approximated as

$$\langle \hat{v}_y \rangle_m \approx \pi \sqrt{2\hat{H}}/b_n \tag{23}$$

Equation (23) is shown as the horizontal dashed lines in Figures 9a–9c. Furthermore, we assume that the incoming and outgoing pitch-angles are equal, a condition which has been shown to be nearly the case for Speiser-type orbits [18]. Equating (23) with two times (22) (to account for both the incoming and outgoing diamagnetic contributions), it is easily shown that β_c is a solution to the equation

$$\frac{8\, b_z \sin\beta_c}{\pi\sqrt{1+{b_z}^2}} \sum_{k=0}^{K} \sqrt{1-\left(\frac{2\pi k b_z \cot\beta_c}{\sqrt{1+{b_z}^2}}\right)^2} = 1 \tag{24}$$

In Figure 10, we show a plot of β_c as a function of b_z (•) as given by (24). We also show on the same figure the value of β_c found by using the actual value of $\langle \hat{v}_y \rangle_p$ (i.e., the solid dots in Figures 9a–9c) instead of the approximate value (i.e., the solid lines in Figures 9a–9c). There are two important facets to this figure: the first is that for small values of b_z, the theoretical and numerical values of β_c are in good agreement, the second is that for larger b_z, β_c becomes smaller. This indicates that for an ensemble of particles with random pitch angles the ratio of the meandering motion current to the diamagnetic will be closer to unity for larger values of b_z.

An important conclusion which may be reached from the above discussion is that if the average pitch angle of a source of particles is greater than β_c the diamagnetic current will be larger than the current due to the meandering motion. In such cases, since the net current is in the wrong direction to create the assumed magnetic field reversal, *no self-consistent solutions exist.* In essence the assumption of the self-consistent solution to the magnetic field and the chosen distribution function are mutually exclusive. If on the other hand the average distribution function has a large drift velocity along the field ($v_D > v_{th}$), the average pitch angle is much less the β_c and the diamagnetic contribution to the current is negligible. In this case it is a simple matter to iterate to self-consistent solutions provided that B_y is negligible. [15,18,19,25]. As mentioned above, one must be careful in this regime since B_y is typically non-negligible and grows on a short time scale. In the regime reminiscent of the quiet-time

magnetotail where the field aligned drift is small and the source distribution is nearly isotropic, the average pitch-angle may be close to the critical pitch-angle. Here the diamagnetic current and the meandering motion current are of the same order magnitude and small changes in the distribution function can result in large changes in the self-consistent solutions. Previous attempts to calculate the current sheet structure in the low drift velocity regime [15] found that if the drift velocity is made lower than some critical velocity, then no equilibrium exist. It was also found that larger values of b_z resulted in a larger value of the critical drift velocity. This loss of equilibrium was referred to as the current sheet catastrophe. We believe that what the authors were actually observing was the transition from the regime in which the meandering current is larger than the diamagnetic current to the regime in which the opposite is true.

VI. Numerical Algorithm

In this section we describe the numerical algorithm used to separate the magnetic field into the part due to the plasma diamagnetism and the part due to the actual particle current. The simplest possible technique is to follow the particle guiding center and to evaluate the guiding center drift and the instantaneous value of the magnetic moment of the particle, $\mu = mv_\perp^2/2B$. Here $v_\perp$ refers to the component of the velocity which is perpendicular to the magnetic field, B is the local magnitude of the magnetic field and the direction of μ is antiparallel to the local magnetic field. These quantities are then used to calculate the particle current and the magnetization vector $\mathbf{M}$ of the plasma respectively. (Note that the magnetization vector $\mathbf{M}$ is calculated in same way as our other equilibrium quantities, i.e. we distribute the instantaneous magnetic moment of each particle on a grid and then add them together with the appropriate weightings.) This technique works well in the asymptotic regions where the guiding center is well defined but fails near the midplane where the guiding center is only poorly defined. We therefore use a hybrid model for calculating the equilibrium profiles. In the regions where the guiding center is well defined, we transform to the guiding center coordinates (position and velocity) for distributing the current density, density and magnetic moment onto the grid whereas in regions where the guiding center is not well defined we use the actual particle position and velocity for distributing the current and density onto the grid. (See appendix B for the calculation of the guiding center location.) This method requires that we follow the actual particle motion in both regions, so that proper phase information is retained for the particle in changing from the magnetized to the unmagnetized regions and *vice versa*. For the case of the magnetotail, the separation between the "magnetized" and "unmagnetized" regions occurs at the separatrix where the particle changes from non-midplane crossing to midplane crossing. In appendix C, we show that the phase space location of the separatrix is approximated by

$$v_z^2 \leq \left[P_y/M - (q/Mc)A_y(x,z)\right]^2 - \left[P_y/M - (q/Mc)A_y(x,z=0)\right]^2. \qquad (25)$$

where A_y is the vector potential for the magnetic field and P_y is the y component of canonical momentum for the particle. The condition given by (24) is simply a statement that for a particle

to be classified as a midplane crossing, the energy in the z-component of the velocity must be larger than the effective potential for the z-motion evaluated at the midplane.

In Figure 11, we show the density, current and magnetic field profiles calculated using the algorithms described in this paper for the case of a Maxwellian with a bulk drift in the tailward direction of 10% of the ion thermal velocity and a high energy isotropic tail; which comprises 10% of the total density. Note that in this case, (which has a nearly isotropic source distribution) the diamagnetization accounts is approximately 80% of the magnetic field due to the particle currents. In Figure 12 we show the same plots but using a Maxwellian source distribution which has a tailward drift of twice the ion thermal velocity (*i.e.*, a highly field aligned distribution). Note that in this case the plasma diamagnetism is only a small correction to the total magnetic field. One must be careful in interpreting the results in this case; however, since we would expect there to be a rapidly growing B_y field associated with the highly field aligned distribution.

VII. CONCLUSIONS

In this report we have described a technique for calculating density, electric current and pressure in a magnetic field reversed region using a test particle simulation. The essence of the technique is to push a distribution of particles through a model magnetic field which is fixed in both time and space. For each particle the density current and pressure are laid down a on grid. After all of the particle trajectories have been calculated we then calculate the total density, current, pressure and magnetic field profiles that the assumed distribution would produce. We then compare the assumed and the calculated magnetic fields. If the difference between the fields is sufficiently small the simulation is stopped and we check to make sure that global pressure balance is obtained [Eq. (19)]. Otherwise, we mix the assumed and the calculated fields and use the combined field in a new iteration of the test particle code. This technique has proven to be very effective for calculating self-consistent equilibrium structures in complex systems such as the magnetotail because it gives very good spatial resolution using a relatively small number of particles. As discussed above, however, it can only yield information regarding time evolution in the sense of a series of quasistatic equilibria.

Using this method we have calculated self-consistent solutions for the equilibrium structure of the Earth's magnetotail during quiet-times which are in good agreement with structures observed in satellite data. An interesting aspect of the solutions is the effect of the plasma diamagnetism. Using a post-processing algorithm (Sections V and VI), we have separated the magnetic field into the components due to the plasma diamagnetism, $4\pi\mathbf{M}$, and the part due to the actual particle current, $\mathbf{H}$. We find that if the average pitch-angle of the source distribution is too large, the magnitude of the diamagnetic current is large than the magnitude of the particle current and in the wrong direction to produce the assumed field reversal. Obviously, in such cases the two assumptions, *i.e.*, the assumed form of the distribution function and the assumed magnetic field structure, are mutually exclusive and no self-consistent solutions exist. We

further showed that for larger values of b_z the average pitch angle required for the existence of self-consistent solutions becomes smaller, *i.e.* we require a more field aligned distribution function. We believe that these results explain the reported "current sheet catastrophe" in Reference [15].

ACKNOWLEDGEMENTS

The authors gratefully acknowledge many helpful discussions with Dr. Glenn Joyce, Dr. Peter Cargill and Dr. James Harold This work was supported by NASA (W-16,991) and ONR. A portion of this work was done while D. L. Holland was a National Research Council Research Associate.

REFERENCES

1. T. W. Speiser, *J. Geophys. Res.*, **70**, 4219, (1965).
2. J. Chen, and P. J. Palmadesso, *J. Geophys. Res.*, **91**, 1499, (1986). (Correction, *J. Geophys. Res.*,**91**, 9025, (1986.))
3. J. Chen, J. L. Rexford, and Y. C. Lee, *Geophys. Res. Lett.*, **17**, 1049, (1990c).
4. R. F. Martin, *J. Geophys. Res.*, **91**, 11,985, (1986).
5. D. B. Curran, C. K. Goertz, and T. A. Whelan, *Geophys. Res. Lett.*, **14**, 99, (1987).
6. T. W. Speiser, D. J. Williams, and H. A. Garcia, *J. Geophys. Res.*, **86**, 723, (1981).
7. L. R. Lyons, and T. W. Speiser, *J. Geophys. Res.*, **87**, 2276, (1982).
8. D. B. Curran, and C. K. Goertz, *J. Geophys. Res.*, **94**, 11,521, (1989).
9. R. F. Martin, and T. W. Speiser, *J. Geophys. Res.*, **93**, 11,521, (1988).
10. J. Chen, G. R. Burkhart, and C. Y. Huang, *Geophys. Res. Lett., 17*, 2237, (1990a).
11. J. Chen, H. G. Mitchell, and P. J. Palmadesso, *J. Geophys. Res.*, **95**, 15,141, (1990b).
12. G. R. Burkhart, and J. Chen, *J. Geophys. Res.*, **96**, 14,033, (1991).
13. G. R. Burkhart, G. R., J. F. Drake, and J. Chen, *J. Geophys. Res.*, **95**, 18,833, (1990).
14. G. R. Burkhart, J. F. Drake, and J. Chen, *J. Geophys. Res.*, **96**, 11,539, (1991).
15. G. R. Burkhart, J. F. Drake, P. B. Dusenbery and T. W. Speiser, *J. Geophys. Res.*, **97**, 13,799, 1992.
16. B. U. O. Sonnerup, *J. Geophys. Res.*, **76**, 8211, (1971).
17. J. Chen, *J. Geophys. Res.*, **97**, 15,011, (1992) .
18. P. L. Pritchett and F. V. Coroniti, *J. Geophys. Res.*, **97**, 16,773, (1992) .
19. Holland, D. L., and J. Chen, *Geophys. Res. Lett., 20*, 1775, 1993.
20. J. Dawson, *Rev. Mod. Phys.*, **55**, 403, (1983) .
21. Pritchett, P. L., and F. V. Coroniti, *J. Geophys. Res., 98*, 15355, 1993.
22. Burkhart, G. R., P. B. Dusenbery, T. W. Speiser, and R. E. Lopez, *J. Geophys. Res., 98*, 21373, 1993.
23. Cargill, P. J., J. Chen and J. B. Harold, *Geophys. Res. Lett., 21*, 2251, 1994.
24. D. L. Holland and J. Chen, *Geophys. Res. Lett.*, **19**, 1231, (1992) .
25. J. W. Eastwood, *Planet. Space Sci.*, **30**, 1641, (1974) .

APPENDIX A

An interesting feature of the results presented in this paper is that as the particle distribution function becomes more isotropic (less field aligned), the diamagnetic contribution to the total cross-tail current becomes larger and that in extreme cases it is large enough to cancel the cross-tail current due to the "meandering motion" of the ions as they cross the midplane. Obviously, in these extreme cases, the assumption of a magnetic field reversed topology and the assumed distribution function are mutually exclusive, since the calculated current is either zero or in the wrong direction to produce the desired field reversal. It is also observed that a larger field aligned anisotropy is required for convergence for larger values of b_z than for smaller values of b_z. It is the aim of this appendix to given a theoretical estimate of the effects of pitch angle and b_z on the diamagnetic current.

Since the net diamagnetic current of a particle in a closed system must be zero, we may calculate the net diamagnetic current that any given particle deposits in the vicinity of the midplane by examining the diamagnetic current that a particle deposits as it enters and leaves the system. In practice, rather than calculating the actual cross-tail current density, we calculate the net y-velocity an ion deposits as it passes through the calculation region. Whereas these only differ by a normalization factor, it greatly simplifies the analysis.

To determine the net positive y-velocity, $\langle \hat{v}_y \rangle$, a particle deposits around the point where it is launched into the system and the point where it escapes from the system we need to calculate the z-position, the z-velocity and the y-velocity as a function of time. In terms of our normalized units, $\hat{z} = z/L$, $\hat{v}_z = v_z/(\Omega_0 L)$, and $\hat{v}_y = v_y/(\Omega_0 L)$ these are given by

$$\hat{z} = \hat{z}_0 + \sqrt{\frac{2\hat{H}}{1+b_z{}^2}}\left[b_z\tau\cos\beta + \frac{1}{\sqrt{1+b_z{}^2}}\sin\beta\sin\left(\sqrt{1+b_z{}^2}\,\tau\right)\right] \tag{A1}$$

$$\hat{v}_z = \sqrt{\frac{2\hat{H}}{1+b_z{}^2}}\left[b_z\cos\beta + \sin\beta\cos\left(\sqrt{1+b_z{}^2}\,\tau\right)\right] \tag{A2}$$

$$\hat{v}_y = \sqrt{2\hat{H}}\sin\beta\,\sin\left(\sqrt{1+b_z{}^2}\,\tau\right) \tag{A3}$$

where $\hat{H} = (mv^2/2)/(m\Omega_0{}^2L^2)$ is the normalized energy, $\hat{r} = r/L$ is the normalized position, β is the pitch angle of the particle, and $b_z = B_n/B_0$ is the ratio of the constant z-component of the magnetic field with the asymptotic value of the x-component of the magnetic field.

During a single excursion of the particle above the $\hat{z} = \hat{z}_0$ plane, we add to the net y-velocity in this region, $\langle \hat{v}_y \rangle_p$, an amount

$$\langle \hat{v}_{yk} \rangle = \int_{\tau_{2k}}^{\tau_{2k+1}} \sqrt{2\hat{H}}\,\sin\beta\,\sin\left(\sqrt{1+b_z{}^2}\,\tau\right)\,d\tau \tag{A4}$$

where τ_{2k}, and τ_{2k+1}, are the times at which the particle cross into and out of the region $\hat{z} \geq \hat{z}_0$ respectively. In actuality, this implies that τ_{2k} and τ_{2k+1} should be two consecutive solutions to the nonlinear equation

$$b_z\tau\cos\beta + \frac{1}{\sqrt{1+b_z{}^2}}\sin\beta\sin\left(\sqrt{1+b_z{}^2}\,\tau\right) = 0 \tag{A5}$$

Rather than solve (A5) for each excursion of the particle above the $\hat{z} = \hat{z}_0$ plane, we hold the position of the guiding center constant in performing the integration. We then shift the location of the guiding center down by an amount, $\Delta\hat{z}$, equal to what it would drift in a complete cyclotron period. This allow us to obtain approximate analytic values for the time limits in the integration. The shift in the $\hat{z}$ location between two successive integration is given by

$$\Delta\hat{z} = \frac{2\pi b_z}{1+b_z{}^2}\sqrt{2\hat{H}}\cos\beta \tag{A6}$$

Note that if $K\Delta\hat{z} > \hat{R}_g$, where K is an integer and $\hat{R}_g$ is the normalized gyroradius of the particle, the particle will not go above the $\hat{z} = \hat{z}_0$ plane and will thus no longer contribute to the net y-velocity deposited in that region. Referring to Figure (13), we see that in a given excursion above the $\hat{z} = \hat{z}_0$, the particles phase angle goes from θ_k to $\pi - \theta_k$ and hence the time integration runs from

$$\tau_{2k} = (1+b_z{}^2)^{-1/2}\left(2\pi k + \theta_k\right) \tag{A7a}$$

to

$$\tau_{2k+1} = (1+b_z{}^2)^{-1/2}\left(2\pi(k+1/2) - \theta_k\right) \tag{A7b}$$

where

$$\theta_k = \sin^{-1}\left[\frac{2\pi k b_z}{\sqrt{1+b_z{}^2}}\cot\beta\right] \tag{A8}$$

Carrying out the integration with the approximate limits, we obtain

$$\langle\hat{v}_{yk}\rangle = \sqrt{\frac{8\hat{H}}{1+b_z{}^2}}\sin\beta\cos\theta_k \tag{A9}$$

or

$$\langle\hat{v}_{yk}\rangle = \sqrt{\frac{8\hat{H}}{1+b_z{}^2}}\sin\beta\sqrt{1-\left(\frac{2\pi k b_z}{\sqrt{1+b_z{}^2}}\cot\beta\right)^2} \tag{A10}$$

The total y-velocity deposited above the $\hat{z} = \hat{z}_0$ plane is found by summing the y-velocity deposited in that region during the individual excursions, i.e.,

$$\langle\hat{v}_y\rangle_{tot} = \sum_{k=1}^{K}\langle\hat{v}_{yk}\rangle. \tag{A11}$$

Here K is the number of excursions that the particle makes above the $\hat{z} = \hat{z}_0$ plane and is given by

$$K = \text{Int}\left[\frac{\sqrt{1+b_z{}^2}}{2\pi b_z}\tan\beta\right]. \tag{A12}$$

Combining equations (A10), (A11), and (A12) yields an expression for the net positive y-velocity deposited above the $\hat{z} = \hat{z}_0$ plane. In addition, we have an equal amount of positive y-velocity deposited symmetrically below the $\hat{z} = \hat{z}_0$ plane. This is because until a particle has drifted at least one gyroradius in the z-direction the negative and positive contributions to the y-current cannot average to zero. Thus, we see that the total y-velocity in the peaks located around the entry and exit points of the particle is given by

$$\langle \hat{v}_y \rangle_p = 2\,\langle \hat{v}_y \rangle_{tot}. \tag{A13}$$

In Figure 9 we show the total y-velocity in the current peaks as a function of the pitch angle as given by given by (A13) (solid line) and as determined by numerically "pushing the particle" through the field (•). As can be seen, the agreement is quite good. One notes, however, that the location of the "breaks" in the curves, which occur whenever the particle is able to add an additional excursion above the $\hat{z} = \hat{z}_0$ plane, fall in slightly different locations for the theoretical and numerically determined results. For the theoretical curves, the breaks in the curves occur at those pitch-angles for which the particle is able to make an additional excursion above the $\hat{z} = \hat{z}_0$ plane, i.e. when

$$\beta_k = \tan^{-1}\left[\frac{2\pi k b_z}{\sqrt{1+b_z{}^2}}\right]. \tag{A14}$$

In actuality, the breaks in the curve occur at those pitch angles for which (A5) picks up two additional roots. This happens whenever the amplitude of the sinusoidal variation in τ becomes sufficiently large that an additional peak intersects the linear term in (A5). Again, the actual values require a solution to the full nonlinear equation. For $k = 0$, this is easily done yielding

$$\beta_0 = \tan^{-1}(b_z). \tag{A15}$$

It is important to note that for predominantly field aligned orbits, i.e., those with pitch angles less than β_0 as given by (A15) there are no solutions to (A5) thus indicating that there is no net y-velocity deposited above the $\hat{z} = \hat{z}_0$ plane. Note that for pitch-angles less than β_0 as given by (A15) the numerically determined points in Figures 9a–9c are all zero. For the other roots the solution is not as simple. As a lowest order approximation to the actual solutions we may approximate the roots as occurring whenever the amplitude of the sinusoidal term in (A5) is equal to the value of the linear term at the points $\sqrt{1+b_z{}^2}\tau = (4k+1)\pi/2$. This yields the values of β_k given by

$$\beta_k = \tan^{-1}\left[\left(2k+\frac{1}{2}\right)\pi b_z\right]. \qquad (A16)$$

In actuality, the solutions occur for values of τ less than this and thus the values of β_k are slightly off. Referring to Figure 14, however, where we have plotted the linear term in (A5) along with three examples of the sinusoidal term with amplitudes given by (a) β_0 as given by (A15) and (b)β_1 and (c) β_2 as given by (A16) we see that (A16) gives an excellent approximation to the actual value of β_k. Comparing equations (A14) and (A16) we see that there is a small positive shift in the actual location of the β_k over the approximate location.

APPENDIX B

In this appendix we explicitly write out the transformation between the actual particle position and the guiding center position for magnetic fields of the form $\mathbf{B} = B_0 f(z)\hat{\mathbf{x}} + B_z\hat{\mathbf{z}}$. In general, the transformation is given by

$$R_{gc} = \mathbf{r} + \frac{\mathbf{v}\times\mathbf{B}}{(q/Mc)B^2}, \qquad (B1)$$

where $B = [B_0 f(z)]^2 + {B_z}^2$. Using (B1), it is trivial to show that the guiding center coordinates X_{gc}, Y_{gc}, and Z_{gc} are given by

$$X_{gc} = x + \frac{b_z v_y}{\Omega_0[f(z)^2 + {b_z}^2]} \qquad (B2a)$$

$$Y_{gc} = y + \frac{f(z)\, v_z + b_z v_x}{\Omega_0[f(z)^2 + {b_z}^2]} \qquad (B2b)$$

$$Z_{gc} = z + \frac{f(z)\, v_y}{\Omega_0[f(z)^2 + {b_z}^2]} \qquad (B2c)$$

Thus, we see that given the local value of the magnetic field and the instantaneous velocity, it is a simple matter to calculate the instantaneous guiding center position. For unmagnetized motion in the field reversal region, the instantaneous guiding center has little physical significance or practical utility.

APPENDIX C

In sections V and VI, we showed that in order to determine the effects of plasma diamagnetism on the equilibrium structure of the magnetotail we needed to separate the orbit into segments which are midplane crossing and segments which are non-midplane crossing. In the former, when calculating equilibrium profiles we distribute the actual particle positions and velocities onto a grid, whereas in the latter we distribute the guiding center positions and

velocities onto a grid. In this appendix we present an approximate expression for the phase space location where the particle changes its behavior from crossing to non-crossing.

We begin by considering the Hamiltonian of a particle in the modified Harris magnetic field

$$H(x,z,v_x,v_z,P_y) = \frac{1}{2}Mv_z^2 + U(x,z,v_x,P_y) \qquad (C1)$$

where

$$U(x,z,v_x,P_y) = \frac{1}{2}Mv_x^2 + \frac{1}{2}M\left[P_y/M - (q/Mc)A_y(x,z)\right]^2. \qquad (C2)$$

is the effective potential for the z-motion, P_y is the y-component of the canonical momentum and A_y is the vector potential. For the modified Harris magnetic field, A_y may be written as

$$A_y(x,z) = -B_0 L \ln\left[\cosh(z/L)\right] + B_z x \qquad (C3)$$

If $b_z \ll 1$ the oscillations in the z-direction are much faster than the oscillations in the x-direction. As a first approximation, we therefore assume that during a single z-oscillation the values of both v_x and x are constant. This approximation is not strictly valid. Rather, if we take v_x to be a constant we should approximate $x = x_0 + v_x t$. For our purposes, however, we find that the simple approximation is sufficient. This is because the orbits which incur significant error using the standard current calculation technique have large pitch angles and thus small v_x Setting v_x and x constant, the condition that a particle is non axis crossing is given by

$$H(x,z,v_x,v_z,P_y) \leq U(x,z=0,v_x,P_y) \qquad (C4)$$

i.e., the energy of the particle must be grater than the effective potential at the midplane. This criterion is graphically depicted in Figure 15 where we have drawn the effective potential for $(P_y/M - \Omega_n x)/(\Omega_0 L) =$ (a) 1, (b) 0, and (c) -1, and we have defined $\Omega_n = qB_z/Mc$. We have neglected the $Mv_x^2/2$ contribution to the effective potential, since it only provides a constant offset. The dashed lines correspond to orbits of different energies as compared to effective potential (c). Particle A violates the inequality in (C4) and is midplane crossing. Thus we use actual particle coordinates for calculating the equilibrium profiles. Particle C represents a solution to the inequality (C4) and is non-midplane crossing. Thus we would use guiding center coordinates for calculating the equilibrium profiles. Particle B represents the equality condition in (C4) and is at the transition point between crossing and non-crossing motion. Solving (C4) for v_z^2 we find that the condition a particle with given x, z, and v_x is given by

$$v_z^2 \leq \left[P_y/M - (q/Mc)A_y(x,z)\right]^2 - \left[P_y/M - (q/Mc)A_y(x,z=0)\right]^2. \qquad (C5)$$

We note that since we have written C5 without making explicit use of the Harris model of the magnetic field, we may use other field reversal models by simply using the relevant model for A_y provided that the approximations regarding x and v_x are still valid.

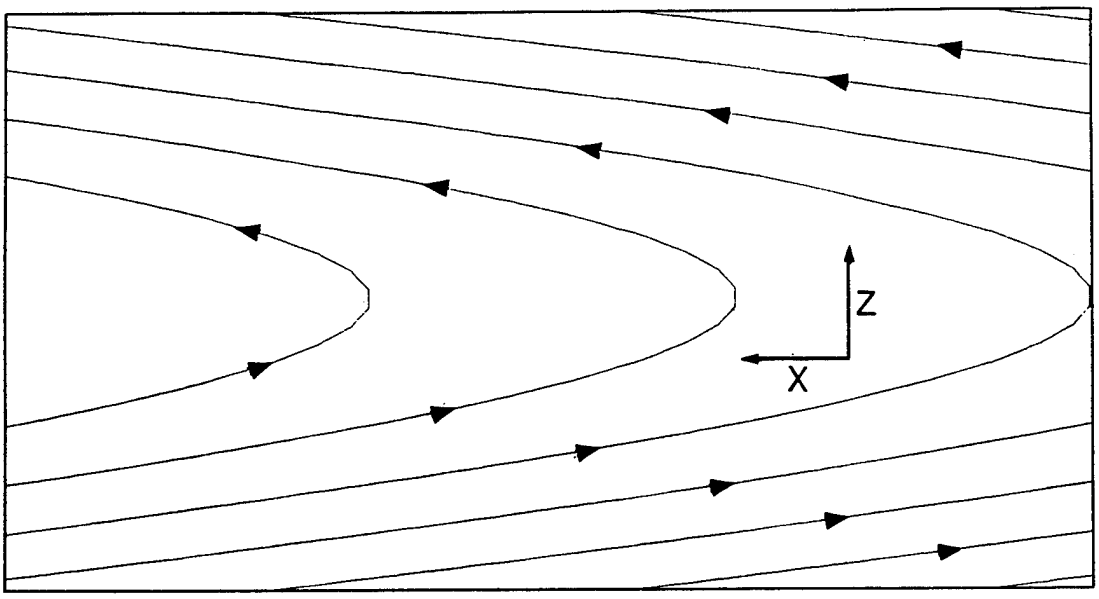

Figure 1: Modified Harris magnetic field geometry

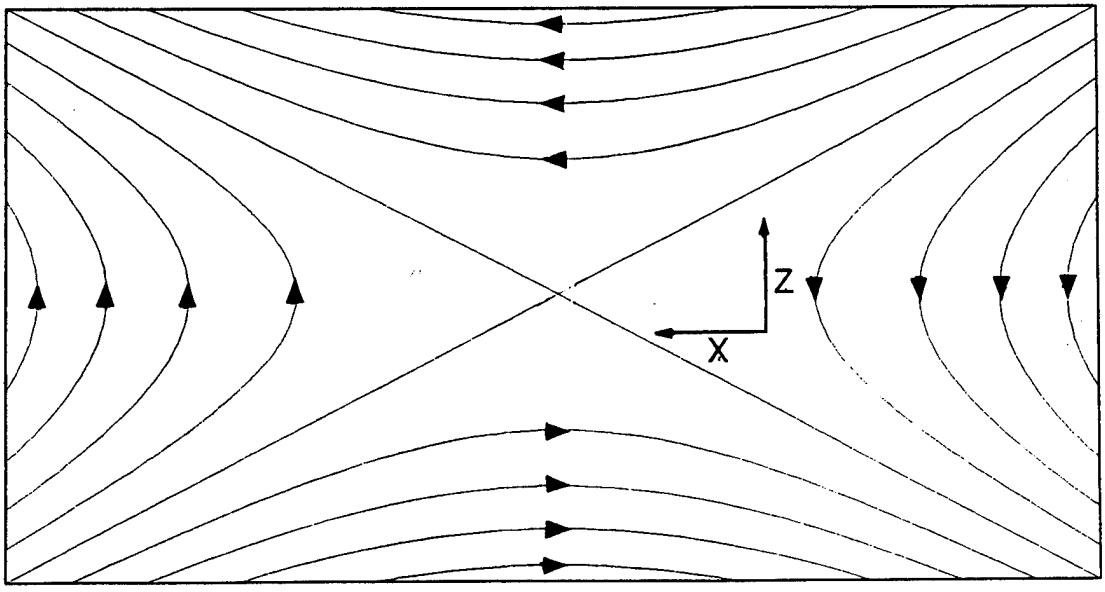

Figure 2: X-line magnetic field geometry

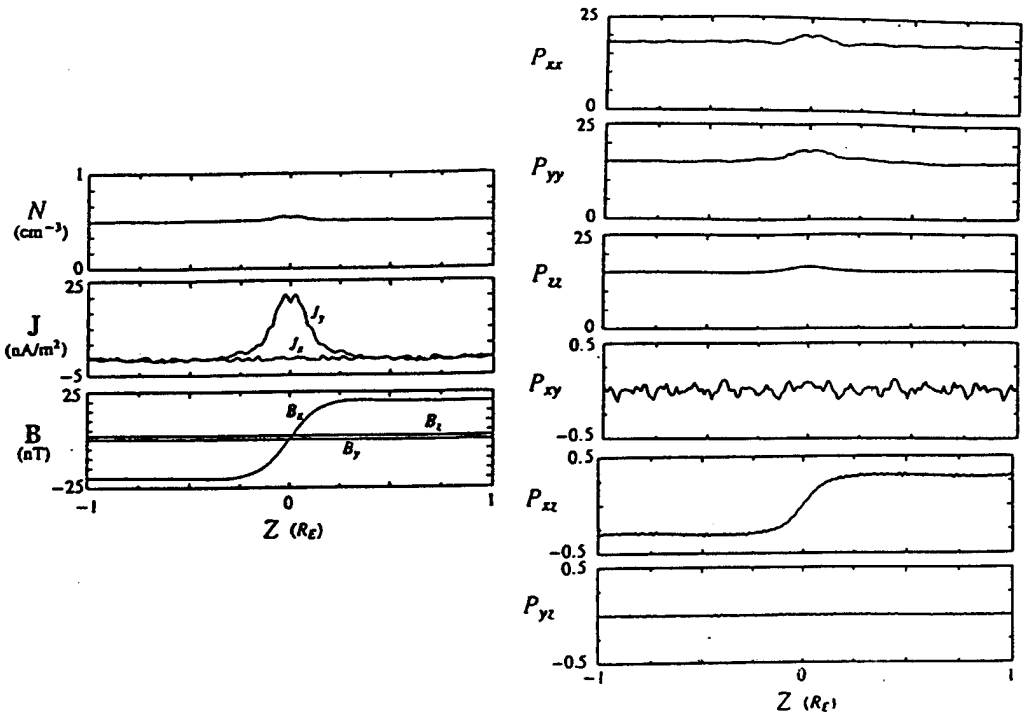

Figure 3. Self-consistent density, current, magnetic field and pressure tensor profiles calculated using a kappa distribution ($\kappa = 4.5$) with a bulk drift in the tailward direction of $v_D = 0.1\, v_{th}$ The units on the pressure tensor elements are nanodyne/cm^2.

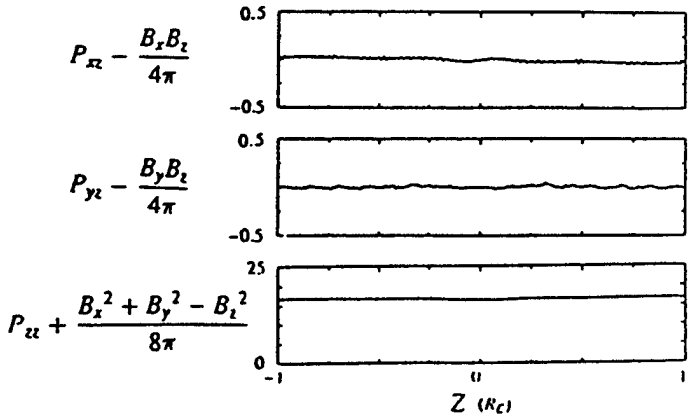

Figure 4. Plot of the left hand side of equations 19 a-c using the results depicted in Figure 3. Since all three curves are essentially flat, we see that pressure balance is maintained to a high degree of accuracy.

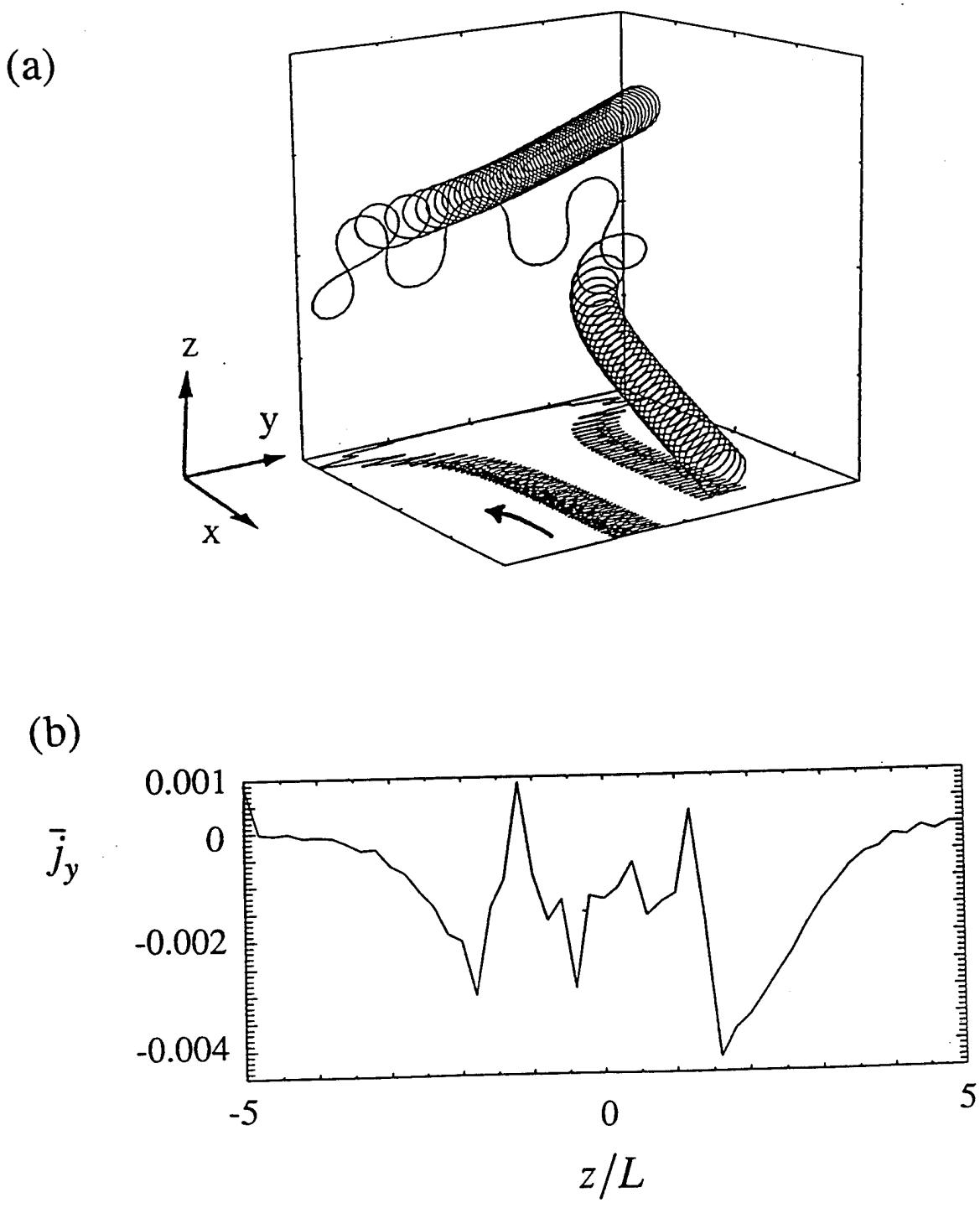

Figure 5: a) Trajectory of an ion with energy $H = 0.24\,L^2\Omega_0{}^2$, initial pitch angle $\beta = 100°$, initial phase angle $\phi = 0°$ and initial starting position $z/L = 6$. b) Current profile of the particle in Fig. 3.*a* as calculated from the standard ridding algorithm with the top grid cell located at $z/L = 5$.

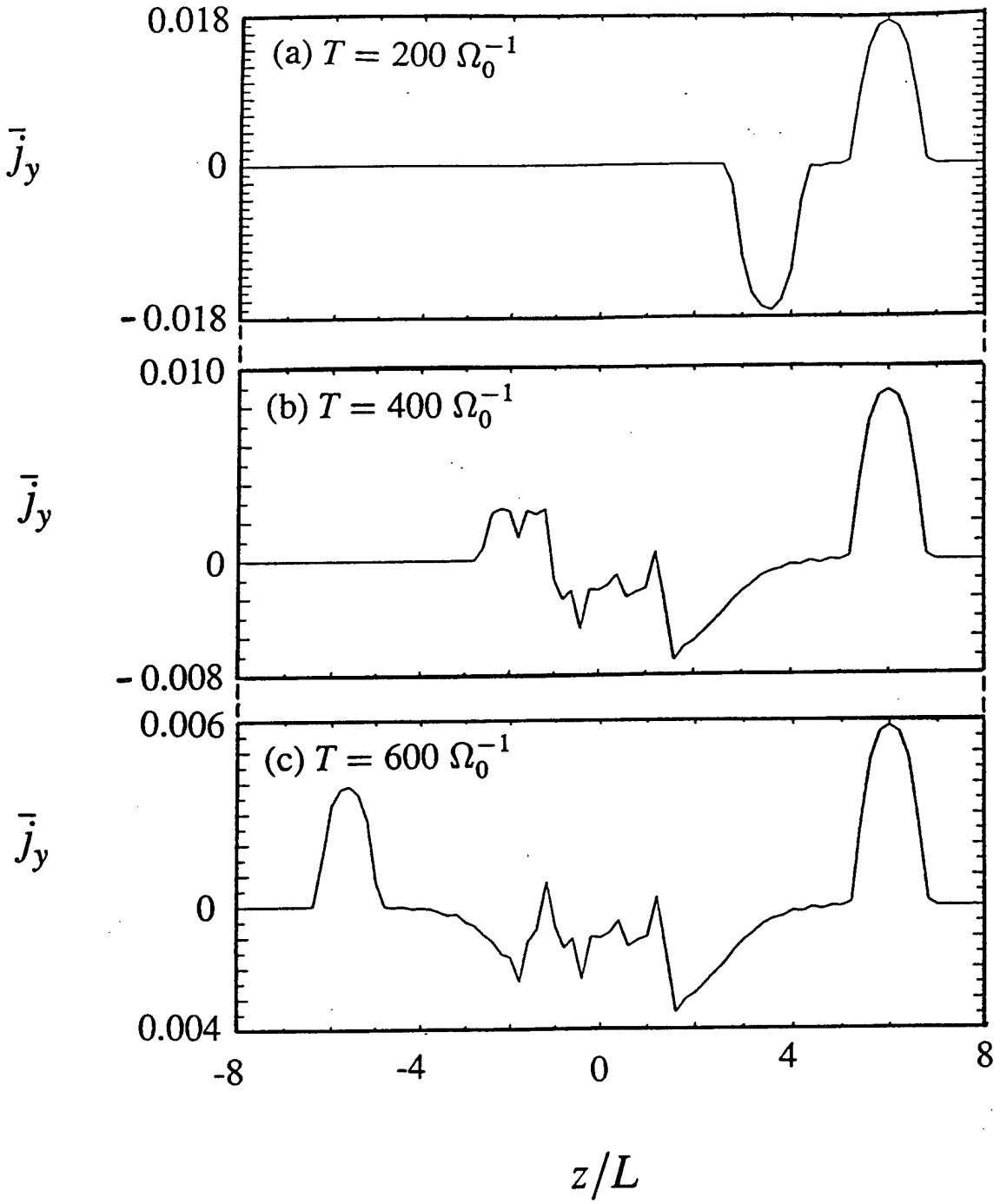

Figure 6: Current profile for the particle in Fig. 5*a* at the three times: a)$T = 200\,\Omega_0^{-1}$, b)$T = 400\,\Omega_0^{-1}$, and c)$T = 600\,\Omega_0^{-1}$. The top grid cell is taken to be $z/L = 8$.

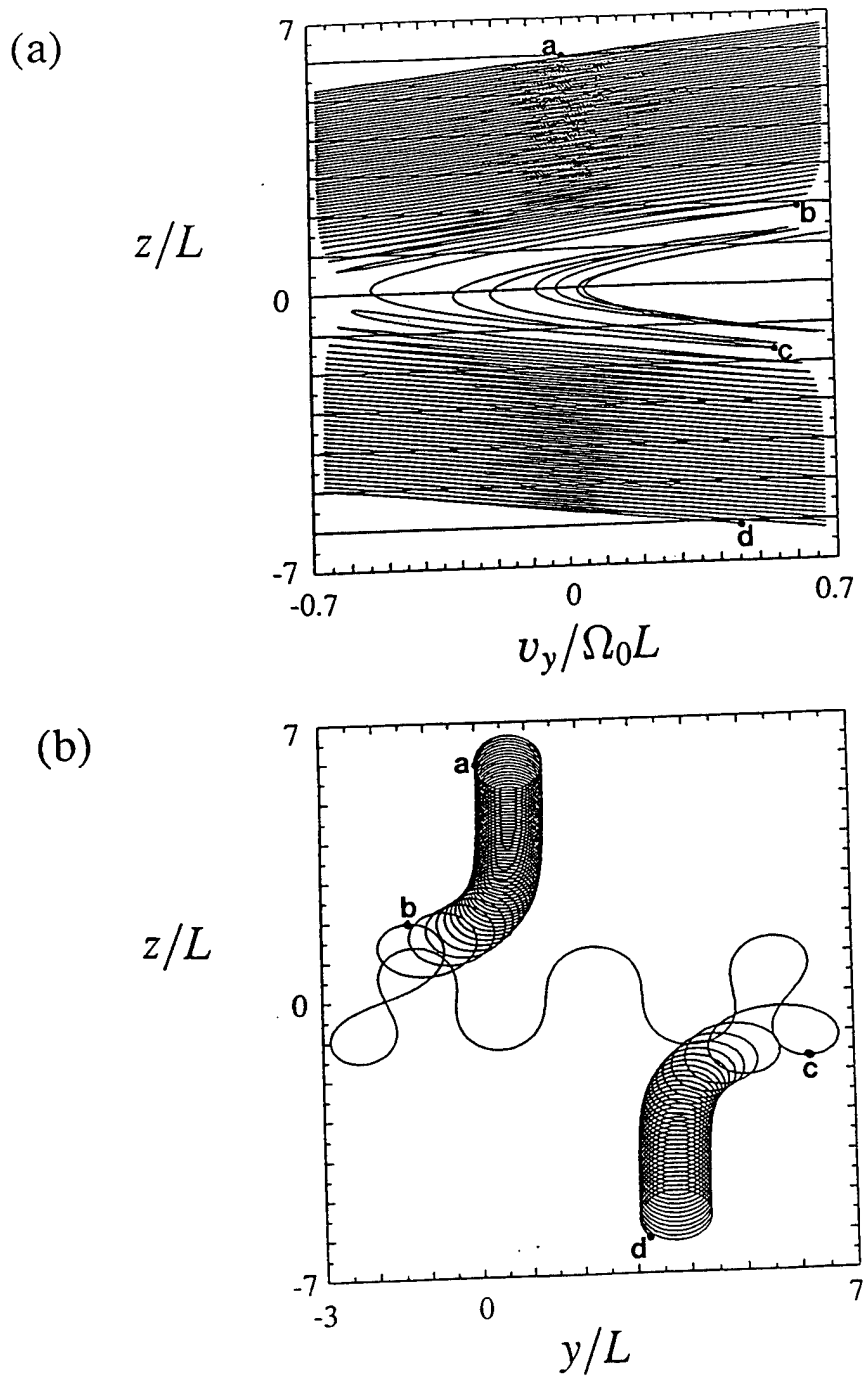

Figure 7: a) $v_y/\Omega_0 L$ as a function of z/L for the particle in Fig. 5*a*. The particle is non midplane crossing on the segments a-b and c-d, and we use guiding center coordinates. The particle is midplane crossing on the segment b-c and we use true particle coordinates. Notes that if actual particle coordinates are used on the segments a-b and c-d, there is an excess of positive y-velocity in the regions $5.3 \leq z/L \leq 6.7$ and $-6.3 \leq z/L - 5$ and an excess of negative y-current in the regions $0.5 \leq z/L \leq 1.9$ and $-2 \leq z/| \leq 0.3$. b) y/L as a function of z/L for the same particle. Note the ∇B drift in the regions around $|z/L| = 2$ and the large y-velocity at $|z/L| = 1$.

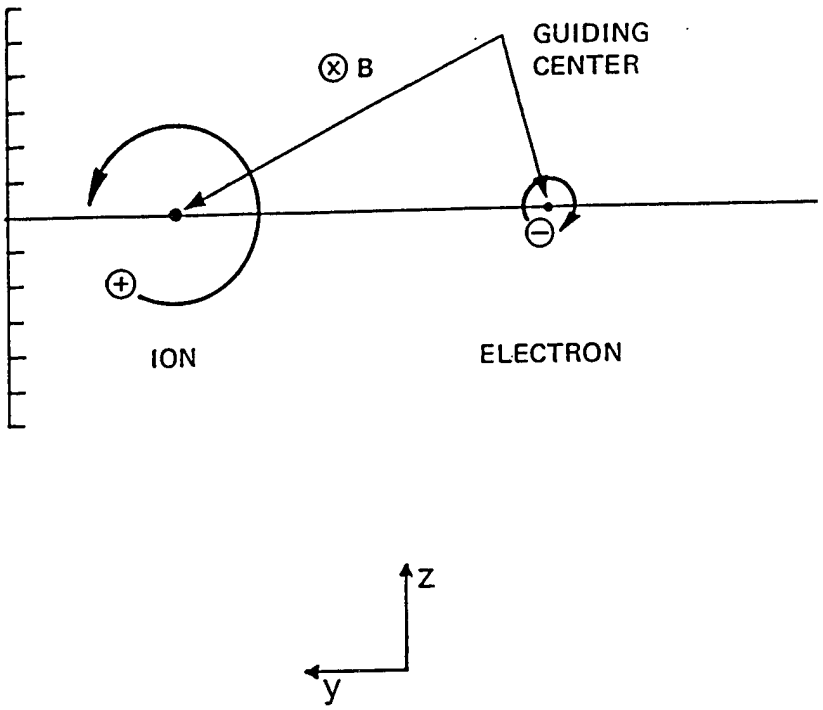

Figure 8: Schematic diagram of ion and electron gyro orbits in a constant magnetic field $\mathbf{B} = B_0\hat{\mathbf{x}}$. Note that above the guiding center the particles have only positive y-current, whereas below the guiding center the particles have only negative y-current

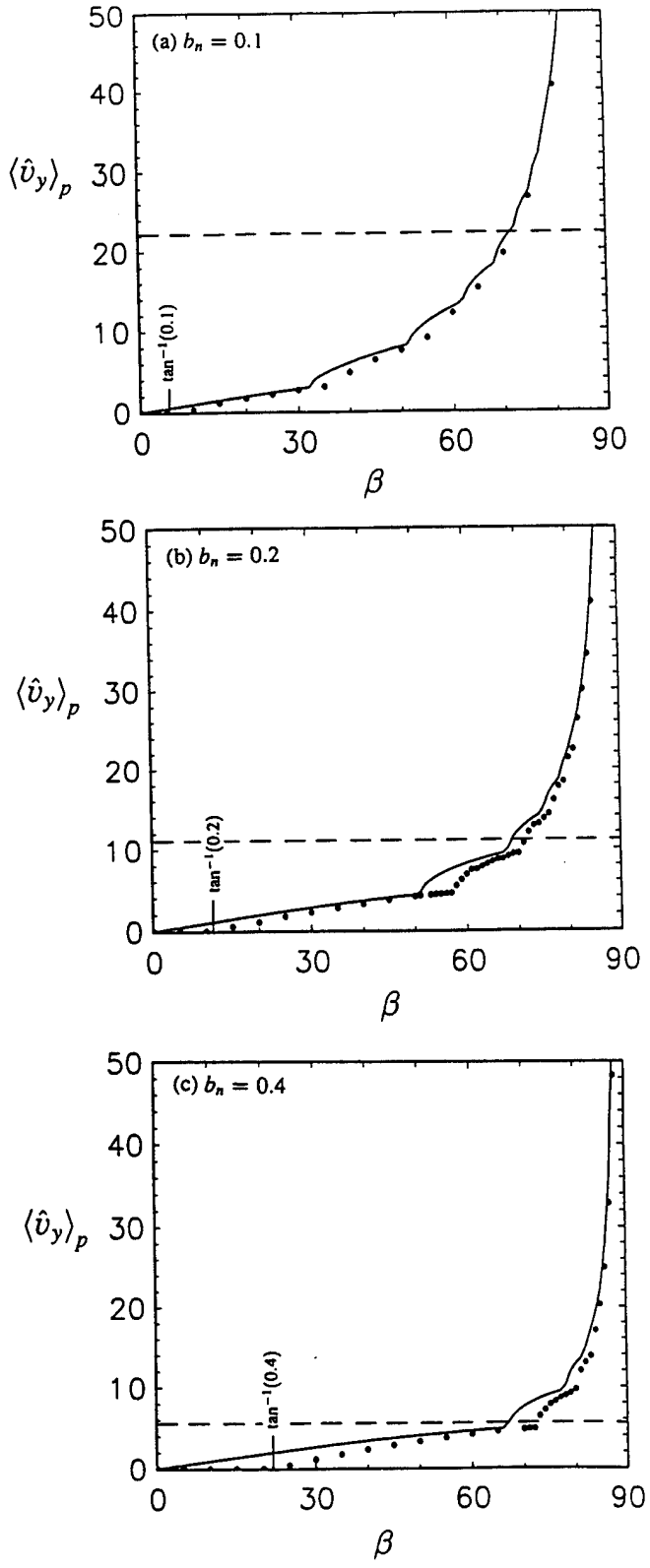

Figure 9: Magnitude of the positive y-velocity deposited near the launching point of the particle as a function of the pitch-angle and for (a) $b_z = 0.1$, (b) $b_z = 0.2$ and (c) $b_z = 0.4$. The solid line is the approximate expression given by (22a) and (22b). The dots are found by pushing the particles through the magnetic field. The dashed vertical lines indicate the pitch-angle that below which there is no net positive velocity left at the launching point.

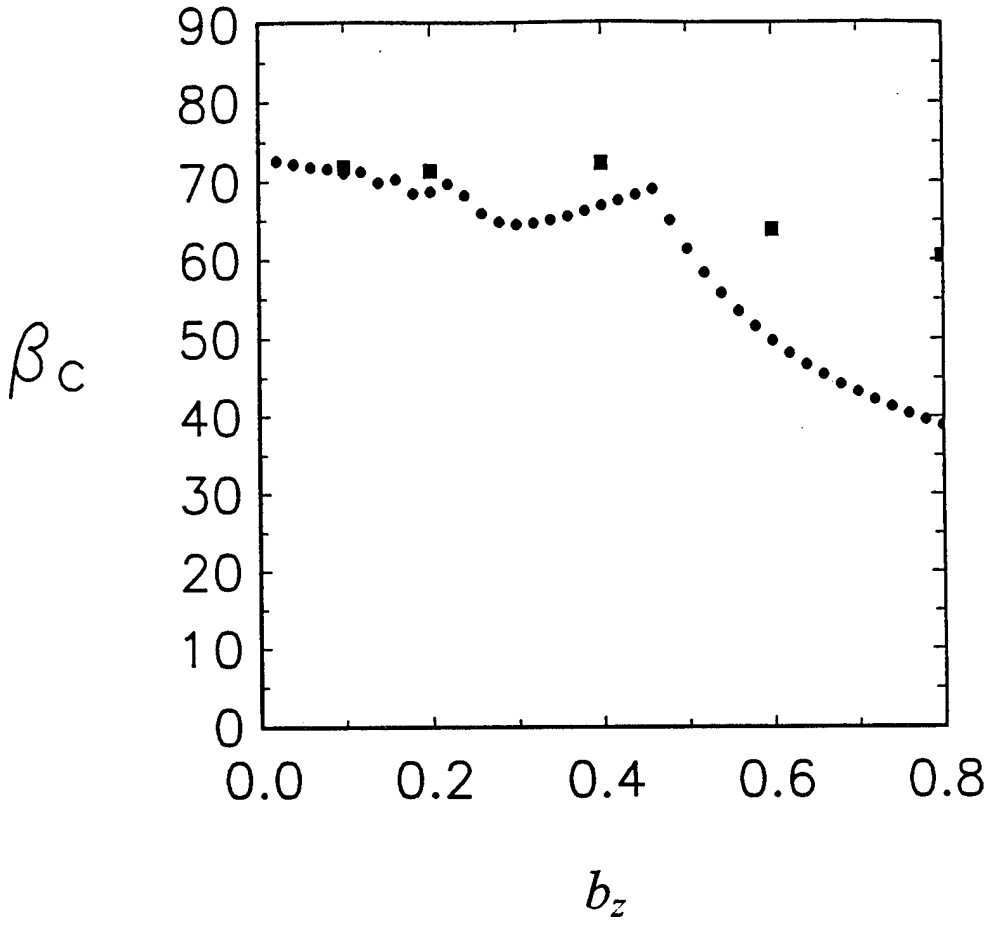

Figure 10: Plot of the critical pitch-angle β_c for which the error current at the midplane equals the meandering current at the midplane as a function of b_z as calculated from Eq. 24 (•). The other points (■) are calculated using the numerically determined values of $\langle \hat{v}_y \rangle_p$.

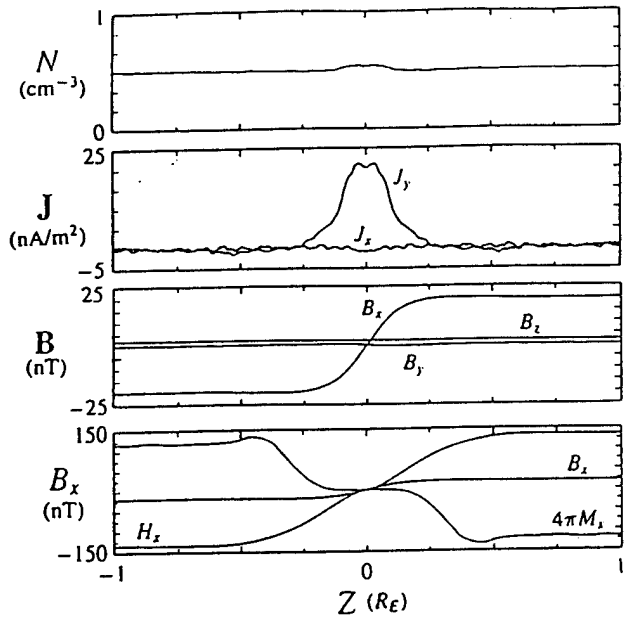

Figure 11. Self-consistent density, current and magnetic field profiles calculated using a Maxwellian with a bulk drift in the tailward direction of $v_D = 0.1\, v_{th}$ and a high energy isotropic tail which comprises 10 percent of the total density.

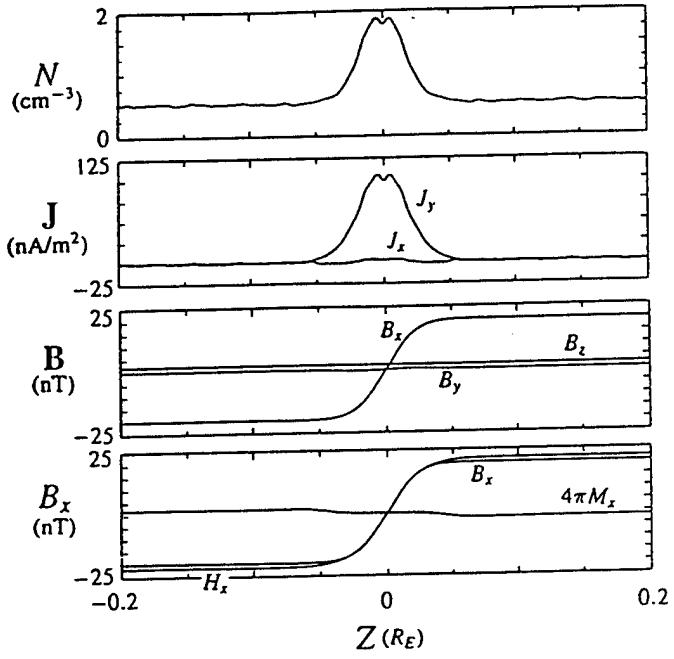

Figure 12. Self-consistent density, current and magnetic field profiles calculated using a Maxwellian source distribution of particles with a bulk drift in the tailward direction of $v_D = 2\, v_{th}$.

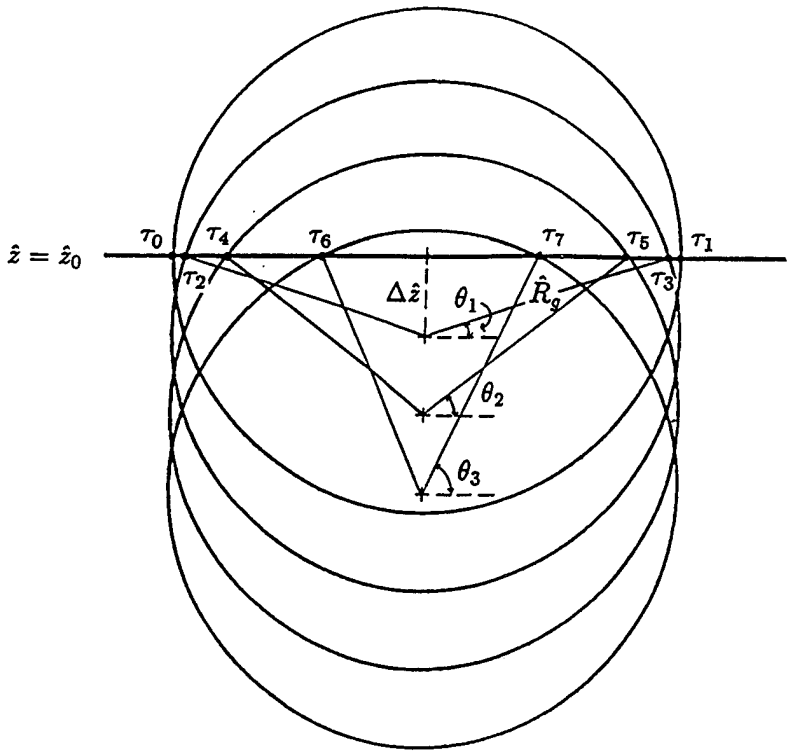

Figure 13: Approximate particle orbits used in deriving Eq. (A.9-A.11)

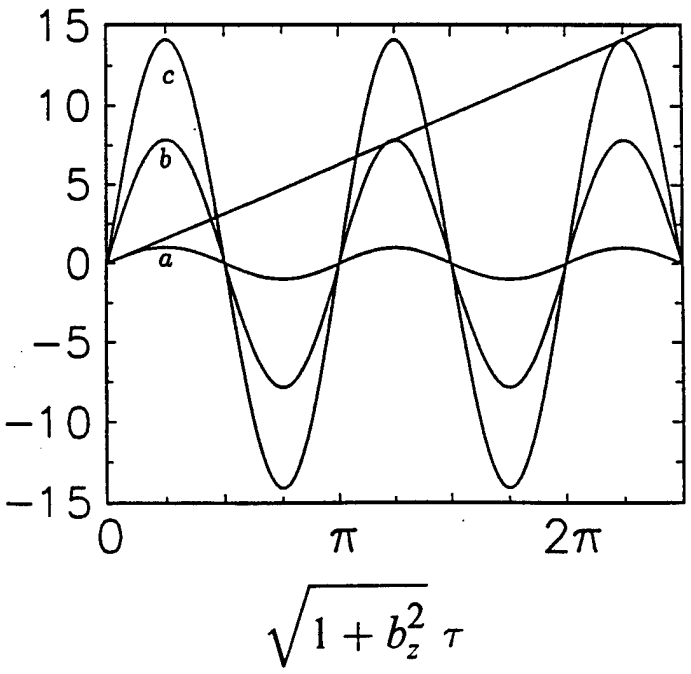

Figure 14: Plot showing graphical solution to equation (A.5). Two new roots to the equation occur when the amplitude of the sinusoidal oscillation $b_z^{-1}\tan(\beta_k)\,\sin\left(\sqrt{1+b_z{}^2}\,\tau\right)$ increases sufficiently to cross the line $\sqrt{1+b_z{}^2}\,\tau$. The curve depicted are for (a) $\beta_k = \tan^{-1}(b_z)$, (b) $\beta_k = \tan^{-1}(5\pi b_z/2)$, and (c) $\beta_k = \tan^{-1}(9\pi b_z/2)$.

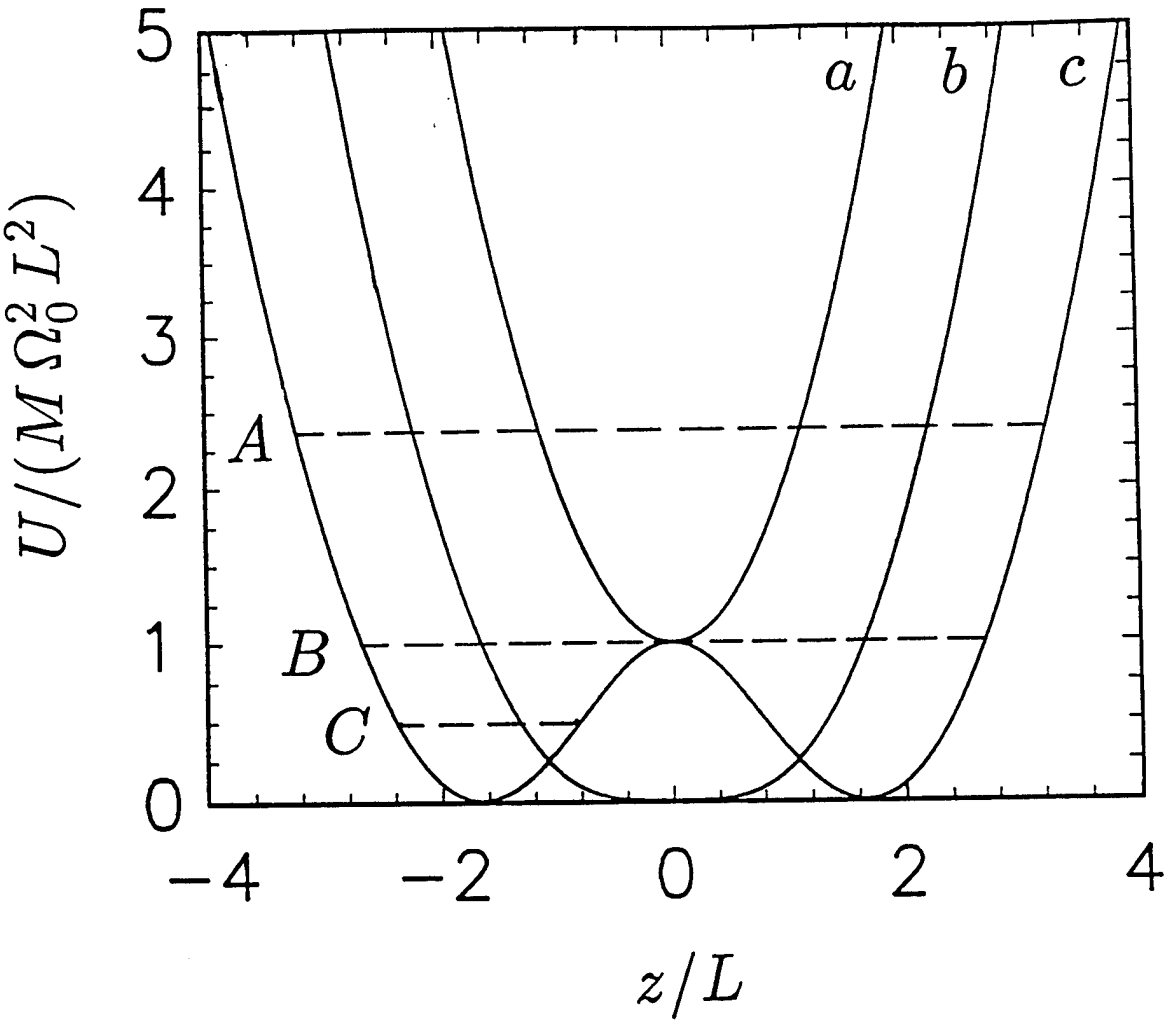

Figure 15: Effective potential for the z-motion for $(P_y/M - \Omega_n x)/(\Omega_0 L) =$ (a) 1, (b) 0, and (c) -1. The dashed lines correspond to orbits of different energies as compared to effective potential (c). Particle A violates the inequality in ($C4$) and is midplane crossing. Particle C represents a solution to the inequality ($C4$) and is non-midplane. Particle B represents the equality condition in ($C4$) and is at the transition point between crossing and non-crossing motion.